article

Fabrication of various plasmonic nano-aperture platforms with a ~10 nm width

Seong Soo Choi [1,] *, Byung Seong Bae [2], Kyoung Jin Kim [1], Myoug Jin Park [1], Young Min Lee [1], Hyun Tae Kim [3], and Soo Bong Choi [3]

[1] Research Center for Nano-Bio Science, SunMoon University 1; sscpjy2010@gmail.com
[2] School of Electronics and Display Engineering, Hoseo University 2; bsbae3@hoseo.edu
[3] Department of Physics, Incheon National University 3; sbchoi@gmail.com
* Correspondence: sscphy2010@gmail.com; Tel.: +82-10-8330-1987(South Korea.)

Abstract: We fabricated the nano-aperture plasmonic platforms for single molecule detection and other various applications such as infrared thermal emission device. The nano-apertures including the nanopores on the pyramid, and the nano-slits on the Au flat membrane were fabricated using a Ga ion focused ion beam drilling technique, followed by high energy electron beam irradiations dependent upon the electron beam current density. The nanopores with a few nanometer size and the nanoslit array with order of ~ 10^0 nm width were fabricated. Optical characteristics for the various nanoslits were examined dependent upon the slit opening width and sample thickness. The broad emission spectra from the (7x 7) slit array are obtained from spp-mediated emission in the visible and infrared region. A sharp strong infrared emission peak is also obtained due to Au nanoparticle. The fabricated Au platform can be utilized as single molecule sensor and infrared thermal emission device.

Keywords: Au nano-pore, surface plasmon polariton; pyramidal aperture; intraband emission; nanoslit array

1. Introduction

The biological cell counter with an electrical detection technique was invented by Dr. Coulter in 1954 [1]. Due to fast developing nanofabrication technology, the portable-size nanobio device using the electrical detection technique for single molecule analysis has been tested and manufactured. Utilizing the state-of-art IC technology, the optical nanoslits or nano-apertures can be an excellent candidate for the next generation single molecule sensor. However, the tiny nano-aperture with its diameter of ~ 10 nm or less would have negligible optical transmission from Bethe's law; $T \sim (d/\lambda)^4$. Therefore, enhancement of optical intensity should be required either by providing the groove patterns or periodic arrays, or plasmonic hot spot [2-5]. The portable optical detection device for single molecule analysis by using a nanoscale aperture or the nanopore with a ~10 nm diameter or less has yet to be fabricated.

We previously reported fabrication of the nano-aperture surrounded by the periodic patterns on pyramidal probes to improve the low transmittance of light through the nanosize aperture [3-5]. The pyramidal nano-aperture has been found to provide excellent light confinement inside a V-shaped cavity, and an enhanced optical throughput via cavity resonance and nanofocusing [6, 7].

Nanopore formation out on the Au membrane using focused Ga ion beam milling techniques and high energy electron beam techniques has also been reported [3-8]. Upon high energy Ga ion impingement on the sample surface, atomic mixing occurs in the melted region within picoseconds, the ions would diffuse and formation of the nanopore would occur. This phenomenon can be

 doi:10.20944/preprints202010.0099.v1

attributed to the thermal spike model [7]. During high energy ion beam impingements, the pore closing would occur due to creation of stressed viscous surface layer and atomic transport to the pore, or mobile surface atom diffusion to the pore.

We reported fabrication of the nanopore on the Au diffused membrane with its diameter ranging from 10 nm to 3 nm inside the FIB drilled aperture by using various surface modifications [3-4, 6-7]. Under the irradiations of the intense high energy electron beam, diffusion of gold atoms and carbon atoms would occur and form the binary mixture membrane. In addition, during irradiations of the samples by the high intensity electron beam, the tiny Au nano-particles on the diffused membrane would grow and become larger via Ostwald ripening, and experience spinodal decomposition [8].

Growth of Au nanoparticles in nature was reported to have five body structures; the tetrahedron, the cube, the octahedron, the pentagonal dodecahedron, the icosahedron, as proposed by theory of five geometrical body structures in nature by Greek Philosopher, Plato. The faces of Plato's polyhedral are triangles, squares, and pentagons. Later, Kepler was inspired by observing the growth and shape of pomegranate seeds and constructed the highly symmetric rhombic polyhedral [9]. It is reported that the early stages of vacuum-deposited Au film consist of Au particles and clusters with various sizes and shapes such as multiple twin particles (MTP) with a decahedron shape and an icosahedron shape [10–12]. The irregular melting temperature of Au nano-particles or clusters vaccum-deposited on the gold film is dependent upon the size, geometrical shape, and numbers of Au atoms in the cluster through so-called magic numbers [13–15]. Due the fact that smaller particles have larger surface to volume ratio, and the surface atoms have lower binding energy, melting temperature of Au nanoparticle is lower than that of Au bulk, down to a few hundred Celsius for ~ 5 nm diameter Au particle. Au nanoparticles with magic numbers would have melting temperatures close enough to that of Au bulk films.

During electron beam irradiation on the thick specimen, the local temperature rise in the specimen can be easily achieved for high energy electron beam irradiation using FESEM or TEM. Depending upon the viscosity of the heated membrane and the surface tension force, and the vapor pressure of the material, the widening or the closing (shrinking) is expected to occur [3-8, 15, 16]. In addition, considering the fact that the carbon filter membrane consists of periodic layer by layer slit –structure with ~ 5 nm gap, the Au nanopore slit array containing carbon atoms could be an excellent candidate for plasmonic aperture platform. For the nanoscale double slits, it is reported that the surface plasmonic wave from the nanoscale slits can provide the periodic interference phenomena for the TM wave between the nanoscale slits, which reduces or enhances the intensity of the far-field [17 - 19]. With proper control of the the circular aperture pitch and the nanoscale slits separation gap, the enhanced optical intensity can be obtained.

Fabrication of plasmonic nano-pore on pyramid and double nanoscale double slits is previously examined [5,6, 20-22]. Light transmission through the conical type aperture dependent upon the polarization and aperture size for $ka << 1$ is well documented, where k is the wave vector and a is the radius of the circular aperture [23, 24]. Lord Raleigh developed a theory of diffraction by small nano-particle and found that the farfield optical emission profile cannot distinguish the shape of the nano-particle due to the fact that light cannot distinguish the particle for the particle size much smaller than the wavelength [24, 25]. This observation can be applied for the nano-aperture with its size much smaller than the wavelength from Babinet principle [26]. It is also reported that with decreasing the size of the aperture, the diffracted angle becomes larger and the intensity profile becomes broader even with a backward scattering upto ~ 40 % for the conical aperture diameter of 60 nm [23]. Furthermore, for the conical aperture diameter of 60 nm and P-polarized beam, backward scattering of the incident beam from the aperture is theoretically presented by using quasi-multiple

Preprints (www.preprints.org) | NOT PEER-REVIEWED | Posted: 5 October 2020 doi:10.20944/preprints202010.0099.v1

dipole approximation, and can be attributed to a Poynting vector flow along the pyramidal surface of the aperture on the pyramidal apex [24].

Surface plasmon (SPP)-mediated intraband emission with its optical peak at ~ 500 nm and the spp-coupled transmission peaks at ranging from ~600 nm to 800 nm is reported depending upon the size and the thickness of the nano-aperture [27]. The intraband optical peak at 500 nm is shown on the 180 nm thick Au films with and even without a ~250 nm diameter single hole. The broad visible and infrared continuum emission via surface plasmon coupling is also reported [28]. Visible emissions are explained by interband transitions of d-band electrons into the conduction band and the subsequent radiative recombination, and the strong infrared emission is generated by intraband transitions mediated by the strongly confined fields near metal nanostructures (localized surface plasmons). Strongly confined fields near gold nanostructures, localized surface plasmon, generate an emission peak in the infrared region due to intraband transitions between conduction band states [27, 28]. Near-field scattering studies of rough silver films also presented that the field-enhancement predominantly originates from the hot spots and Au nano-particles, and elliptically shaped particles where the presence of local plasmon modes leads to very large field enhancements [28]. A direct intraband optical transition is forbidden in the dipole approximation due to having the same symmetry of the initial and final electronic state. However, the spatial confinement and coupling of the near-field results in an increase of contribution of higher order transition moments, such as the electric quadrupole and octupole moments, and the radiative intraband transitions in conduction band can be allowed to cause the near-infrared emission observation of the nanostructures [28]. Hence, three steps of intraband emission are proposed as follows: (i) local field enhancement would create optical fields with large wave numbers near the surface, (ii) these large wave numbers carry enough momentum to allow direct intraband transitions within the conduction band, (iii) these transitions would couple to plasmon eigen modes of the structure, and the radiative emission would follow [29].

The strongly confined fields near gold nanostructures such as a nano-slit array with a tiny ~ 10 nm opening width, can also generate emission peaks in the infrared region due to the intraband transitions between conduction band states. In addition, near-infrared emission generated by nanoscale slits can be utilized for the far field emitters and possible nearfield thermal cooling [30, 31]. In this report, we will investigate the fabrication of various nano-aperture platforms with the circular-type aperture and the nanoslit type array and the optical characterizations.

2. Materials and Methods

Two types of Au nano-aperture platforms will be designed and fabricated: Nano-aperture array on the pyramid and on flat membrane, and nanoscale slit array platforms. First, we carried out fabrication of nanometric size aperture arrays on top of oxide pyramids using conventional Si microfabrication techniques as in Figure 1(a) – 1(f). In addition, TEM grid samples with (100 μm x 100 μm) SiN membranes were also purchased from TEMwindows Company (www.temwindows.com), followed by the physical vapor deposition of Au thin films and dry etching of the supporting SiN film depending upon the experimental conditions. After bulk Si etching on the backside of the Si wafer using TMAH solution, a (10 x10) oxide pyramidal array is presented in Fig. 1(g) and a side view of the single oxide pyramid is shown in Fig. 1(h). A circular oxide aperture on top of the pyramid is shown. due to stress-dependent oxide growth on the pyramidal apex and a slow isotropic etching of the SiO2 as in Fig. 1(i). Then, a 200 nm Au thin film deposition was performed using a thermal-deposition system, followed by 30 keV focused Ga ion beam (FIB) drilling with Focused Ion beam instrument (FEI Helios NanoLab Dual Beam system) and high energy electron beam irradiations using field emission scanning electron beam microscopy(FESEM) and transmission electron beam microscopy(TEM). Electron beam irradiation techniques such as TEM (JEM-2010 and JEM-3011 HR), FESEM (JSM 6400) were utilized at National Nation Fabrication Center (NNFC) in Daejeon,

Preprints (www.preprints.org) | NOT PEER-REVIEWED | Posted: 5 October 2020 doi:10.20944/preprints202010.0099.v1

Korea. The optical spectra in the visible range were also obtained by using Nikon Optical Eclipse Ti-U microscope with Princeton Instruments spectrophotometer (Acton SpectroPro 2300i, 150g/mm). In addition, a solid state ND: YAG laser system with a wavelength of 532 nm for a light source and a silicon photo sensor with a 15 mm cone attenuated F filter (spectral range: 400 nm ~ 1064 nm) for photo detection using a Witec SNOM instrument were used in the experimental setup. The minimum detection limit is order of 1 nW (~ 8.0×10^{-10} W).

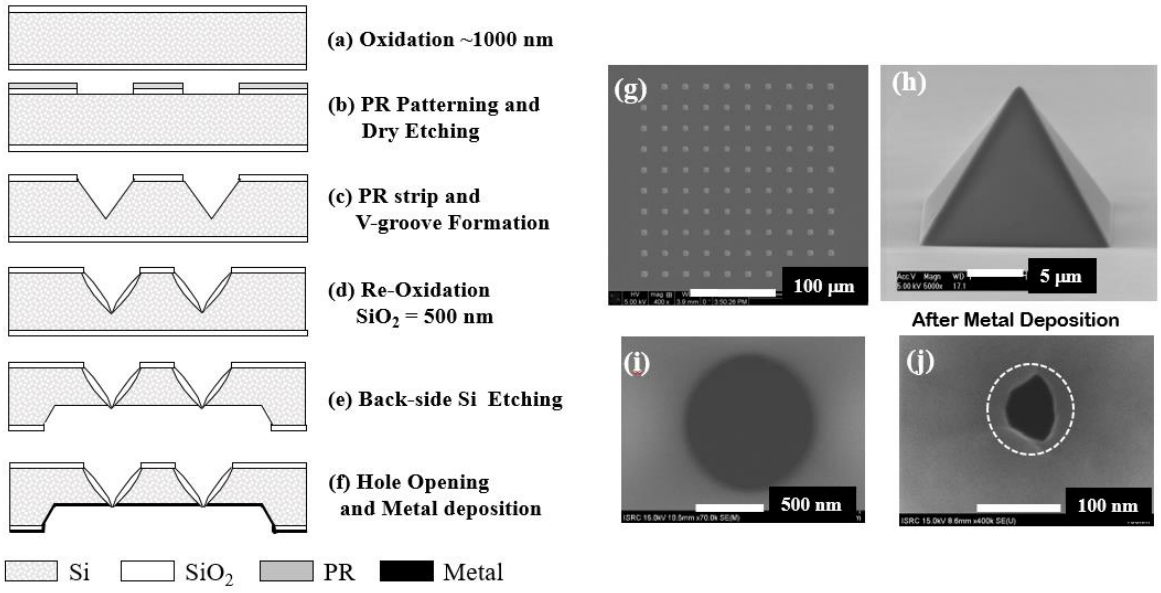

Figure 1. Fabrication schematics for the nano-apertures are shown in Fig (a)-(f). Fig. 1(g) shows the (10x10) pyramidal array, and A FESEM image of the side view of the single pyramid is shown in Fig. 1(h). FESEM images of the circular hole at the top of the pyramid after the TMAH bulk etching is presented in Fig. 1(i), and the nano-aperture is shown after Au thermal deposition in Fig 1(j).

3. Results

We have fabricated the nano-apertures on the flat membrane, and the pyramid deposited by Au thin film, followed by 30 keV Ga ion focused ion beam milling. The Nano-aperture with its diameter 100 nm or less is found to be rather difficult due to instable focused ion beam and other conditions of the system. Hence, gold(Au) apertures with ~ 200 nm or greater are fabricated on the 200 nm thick Au film. In order to reduce the size of the circular-type Au aperture, a 10 second 1.4 nA electron beam irradiation at 2 keV was carried out by using field emission scanning electron beam technique installed at Dual Beam Helio(FEI) was carried out, followed by the high energy electron beam irradiation by using TEM.

3.1. Pore formation process mechanism: Influence of the high energy electron beam irradiation. We have investigated pore formation on the FIB drilled Au aperture under the influence of the high energy electron beam irradiation by using TEM (JEM-2010, JEM-3011 HR). Figure 2(a) shows a nanopore with a 55.75 nm diameter on the gold diffused membrane mixed with carbon atoms after the 2 keV FESEM electron beam irradiation. For the aperture with its diameter greater than aperture thickness, the aperture would not shrink even with high energy electron beam irradiation at 300 keV TEM. However, for electron beam irradiation using FESEM, Au atoms on the surface would diffuse into the aperture, then forms the nanopore on the diffused Au membrane mixed with carbon atoms.

Preprints (www.preprints.org) | NOT PEER-REVIEWED | Posted: 5 October 2020 doi:10.20944/preprints202010.0099.v1

Hence, we applied a two-step process for the pore formation for FIB drilled Au aperture with a ~ 279.5 nm diameter.

- Pore formation on the aperture with its diameter bigger than the aperture thickness.

Figure 3 presents the pore shrinking under the successive electron beam irradiations for 50 minutes. For the 1st and 2nd electron beam irradiations for 10 minutes and 20 minutes, the pore shrinks from 55.75 nm to 30.79 nm, then to 20.97 nm, respectively. However, the pore shrinking rate becomes slower; for 3rd, 4th, and 5th 10 min-electron beam irradiation, from 20.97 nm to 7.96 nm, to 5. 79 nm, and down to 4.20 nm, respectively. Apparently, with decreasing pore size, the shrinking rate for the 5th electron beam irradiation is measured to be ~ 0.159 nm /minute.

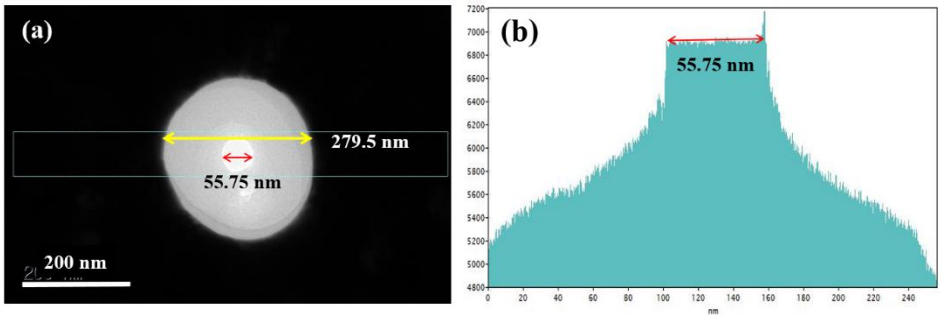

Figure 2. A ~ 279.5 nm diameter circle was initially drilled on a 200 nm thick Au flat film by 30 keV Ga ion beam, followed by high energy electron beam irradiation at 2 keV, 1.4 nA FESEM electron beam irradiation for 10 seconds. A TEM image of the 55.75 nm diameter nanopore on the Au diffused membrane is shown in (a). An electron beam intensity profile at the electron detector displays a 55.75 nm diameter of the formed nanopore on the diffused Au membrane mixed with carbon atoms in (b).

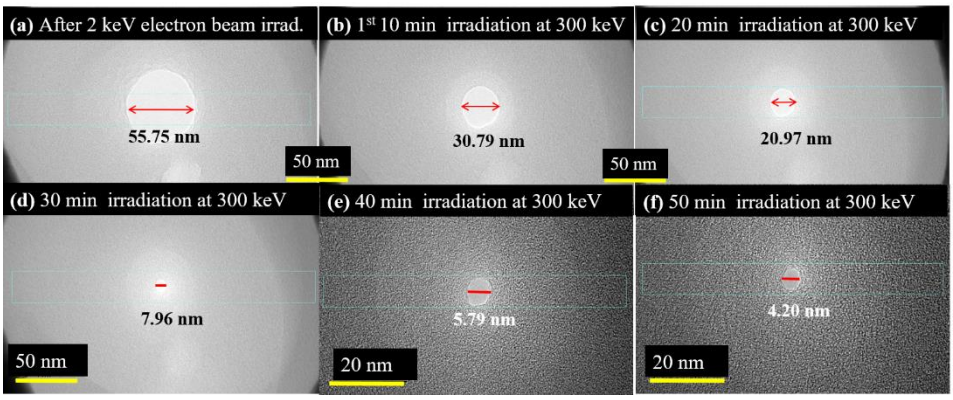

Figure 3. Successive electron beam irradiations with a 10 minute-interval were performed under 3 pA/cm^2 low current density of high energy electron beam irradiation at 300 keV TEM (JEM-3011 HR). A TEM image of a 55.75 nm diameter nanopore on the Au-C diffused membrane is shown in (a). A nanopore with its diameter of 55.75 nm was reduced to a smaller diameter nanopore of 30.79 nm, 20.97 nm, 7.96 nm, 5.79 nm, and 4.20 nm for 10 min, 20 min, 30 mi, 40 min, and 50 min, respectively.

- Pore formation on the aperture with its diameter smaller than the aperture thickness.

Preprints (www.preprints.org) | NOT PEER-REVIEWED | Posted: 5 October 2020 doi:10.20944/preprints202010.0099.v1

The Au aperture with its diameter less than 100 nm for 200 nm thick Au film was fabricated by using 30 keV Ga ion beam milling.

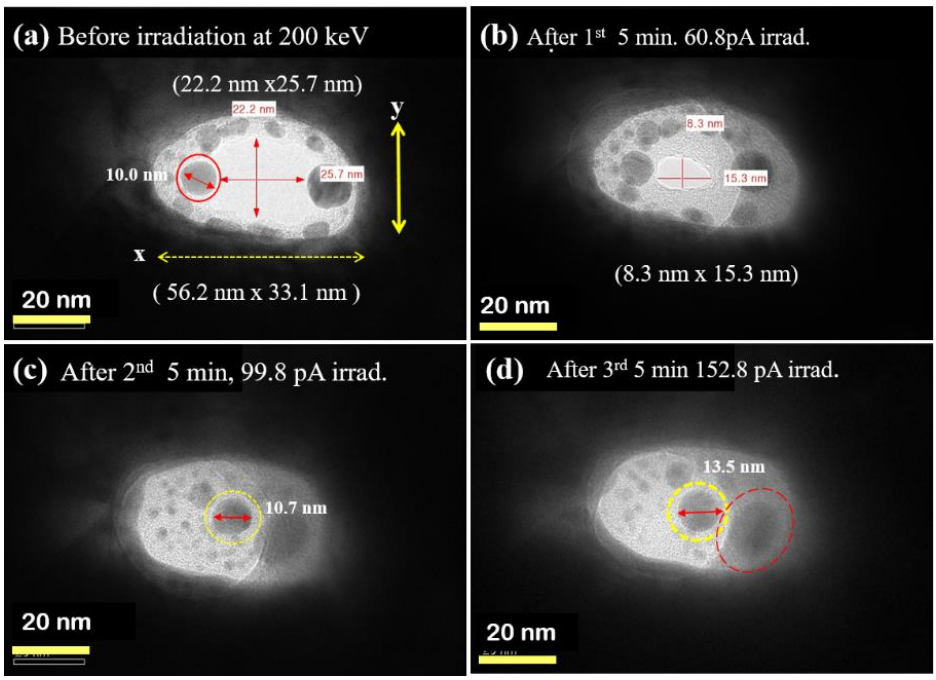

Figure 4. TEM images of a nanopore under high energy electron currents at 200 keV (JEM-2010) are shown. A (56.2 nm x 33.1 nm) size Au aperture before irradiation in (a), Reduced nanopore of (8.3 nm x 15.3 nm) under 1st 60.8 pA electron beam irradiation in (b), a completely closed pore under 2nd 99.8 pA electron beam irradiation (c), thinned pore membrane under the very high intensity 152.8 pA for 5-minute irradiation (d). Several Au nanoparticles were evaporated and thinning of the membrane is also shown in (c) and (d). Under 60.8 pA/cm^2 electron beam irradiation along with diffusion of the 10 nm size Au nanoparticle as shown in (b) and (c).

Figure 4 presents the TEM images under the high energy electron beam irradiation on the FIB drilled Au aperture by using a 200 keV TEM. For a designed diameter of 50 nm, the egg shape aperture (56.2 nm x 33.1 nm) was obtained due to straggling of the focused Ga ion beam drilling process, in addition, a pore size of (22.2 nm x 25.7 nm) on the Au-C mixed membrane was formed inside a drilled Au (56.2 nm x 33.1 nm) aperture. Due to the thermal spike rise during a 30 keV FIB drilling process, diffusion of Au atoms and C atoms occurs simultaneously and forms the thin membrane mixed with gold and carbon atoms, so that several Au particles and clusters on the Au-C diffused membrane are shown. A big Au particles (~ 10 nm diameter size of one particle on the left) (dashed red line) and another one on the right are also shown in (a). After 1st electron beam irradiation with 60.8 pA for 5 minutes, the (22.2 nm x 25.7 nm) pore was reduced to the (8.3 nm x 15.3 nm) pore in Fig. 4(b). After second 99.8 pA irradiation at 200 keV, the pore was completely closed and diffusion of Au particles are clearly shown in Fig. 4(c). After 3rd 152.8 pA electron beam irradiation for 5 minutes, the diffused Au particle (13.5 nm diameter, inside the red dashed circle) became bigger than one before the electron beam irradiation as in Fig 4(a). The diameter of the Au particle (~ 10 nm) before electron beam irradiation in Fig. 4(a) became slightly bigger; the diameter of the Au particle is 13.5 nm as in Fig. 4(d), the diffused membrane became thinner and the small particles became smaller and the big particles became bigger. This phenomenon can be attributed to Ostwald ripening effect. Please note that the large circular type particle (right side in Fig. 4(a)) became an ellipsoidal shape particle (inside the dashed red inside in Fig. 4(d)).

Preprints (www.preprints.org) | NOT PEER-REVIEWED | Posted: 5 October 2020 doi:10.20944/preprints202010.0099.v1

3.2. Optical characteristics for the fabricated nano-aperture platforms: nanoscale double slits and nanopores on pyramid

- Nanoscale double slits dependent upon the slit separation(pitch):

We have carried out preliminary test with fabricated nanoscale double slits with different slit separations. The surface plasmonic waves emanating from the nanoscale slits can provide the periodic interference phenomena for the TM wave between the nanoscale slits, which reduces or enhances the intensity of the far-field [17–19]. With proper controlling the pitch of the aperture and the nanoscale slits separation gap, the enhanced optical intensity can be obtained. Furthermore, considering the fact that fabricating the uniform circular aperture with its diameter smaller than 100 nm is rather challenging and very difficult, and carbon filter membranes consists of slit-type structure with ~ 5 nm separation. Therefore, nanoscale slit type structures formed with an Au-C mixture membrane can be an excellent candidate for the various application including single molecule sensor.

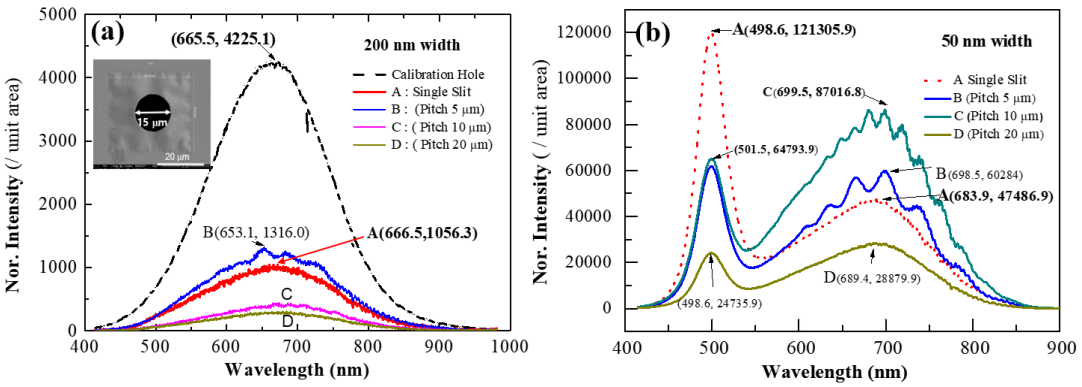

Figure 5. Optical characteristics of nanoscale double slits dependent upon the pitch(slit-separation) are presented. For the input calibration sample with a 15 μm diameter, and all the samples of a 200 nm slit width, the optical peaks around ~ 665.5 nm with the Gaussian profiles are presented in Fig. 1(a). Fig. 1(b) shows two optical peaks: one around ~500 nm and another around~ 700 nm. The transmitted optical intensities from A and B in (a) present the peaks around ~ 666.5 and 653.1, respectively in (a), and the peaks around ~683.9 nm and ~698.5 nm with interference patterns, respectively in (b). For a 200 nm slit width and a 50 nm slit width, the highest transmitted intensities are shown from B in (a) and C in (b).

Figure 5 present the optical characteristics for the nanoscale double slits with a 200 nm slit width and a 50 nm width on 200 nm thick Au membrane. The circular aperture with a 15 μm diameter is fabricated and optically characterized as input beam intensity for calibration. The visible input beam intensity spectrum with its optical peak at 665.2 nm and its range of (400 nm ~950 nm) is shown in Fig. 5(a). For a single slit with a 200 nm width (A) in Fig. 5(a), the output intensity profile with reduced beam intensity and its peak at 666.5 nm is shown. However, for the single slit (A) with a 50 nm slit-width, two optical peaks are presented; one sharp strong peak at 498.6 nm and the other one with much smaller peak at 683.9 nm. All of the double slits with a 200 nm width, there are no optical peaks around ~ 500 nm. However, for the slits with a 50 nm slit width, the largest optical peak at 498.6 nm from the single slit is observed. And the high intensity peaks around ~ 500 nm are shown with periodic intensity modulations between 650 nm and 850 nm from the double slits

Preprints (www.preprints.org) | NOT PEER-REVIEWED | Posted: 5 October 2020 doi:10.20944/preprints202010.0099.v1

with 5 μm pitch and 10 μm pitch in Fig 5(b). These phenomena can be attributed to the surface plasmon polariton mediated intraband emission.

- Nanoslit array on ~ 130 nm thick Au film dependent upon slit width

The four different type optical platforms are fabricated on ~ 130 nm Au film as Figure 6; a (7 x 7) circular type aperture array with a ~ 100 m designed diameter, two (7x7) slit arrays with a (100 nm wide x 500 nm long) slit size, (7x7) slit array with a (~ 40 nm wide x 500 nm long) slit size. The (x, y) pitch of the circular type aperture and the slit array is designed to be (1μm, 1 μm) and (550 nm, 500 nm), in Fig. 6(a) and Fig. (b), respectively. The measured pitch for the slit array pitch is found to be (~ 532 nm, ~471 nm) in Fig. 6(b). The ~ 10 nm wide membrane with Au clusters and particles during Ga ion beam milling is shown in Fig. 6(c). The corresponding electronic profile for the width of the slit is shown in Fig. 6(c) and (d).

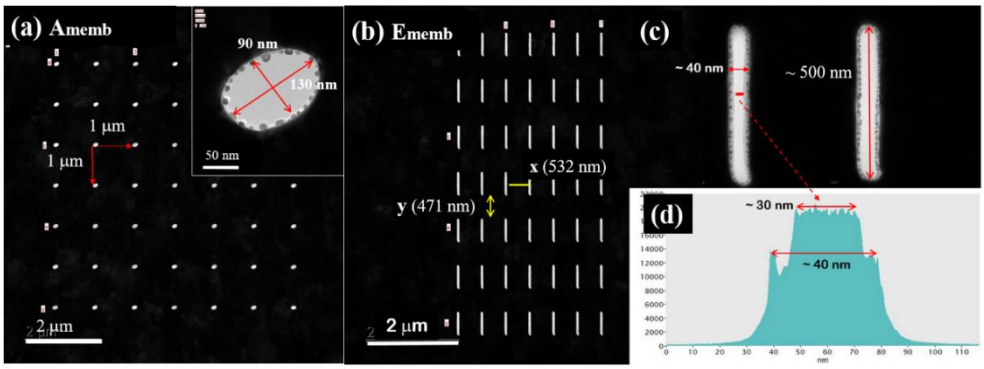

Figure 6. TEM images for the circular type aperture with its size of (130 nm x90 nm) and nanoscale slit array of its size (~ 40 nm wide x ~500 nm long) are shown. The (x, y) pitches of the (7 x 7) circular type array and (7x7) nanoslit array is (~ 1μm x 1 μm) and (532 nm x 471 nm), respectively. The TEM image of the nanoslit and the corresponding electronic profile are presented in (c) and (d).

Figure 7 presents the optical emission profiles from 4 nano-aperture platforms. All four nano-apertures have sharp optical spectra centered around ~500 nm, possible due to the spp-mediated intraband emission. The two (7 x 7) nanoslit arrays with a 100 nm width (G membrane and H membrane) present the exactly identical small spp-coupled transmission peaks centered around ~ 671.5 nm. However, the nanoslit array with a ~ 40 nm width (F membrane) is observed to be a smaller shoulder profile around ~665 nm than those from (G and H). The optical emission profile from A membrane with a (7 x7) circular type array with a (~130 nm x ~90 nm) aperture presents a sharp emission peak at ~500 nm with a negligible shoulder at 650 nm.

Preprints (www.preprints.org) | NOT PEER-REVIEWED | Posted: 5 October 2020 doi:10.20944/preprints202010.0099.v1

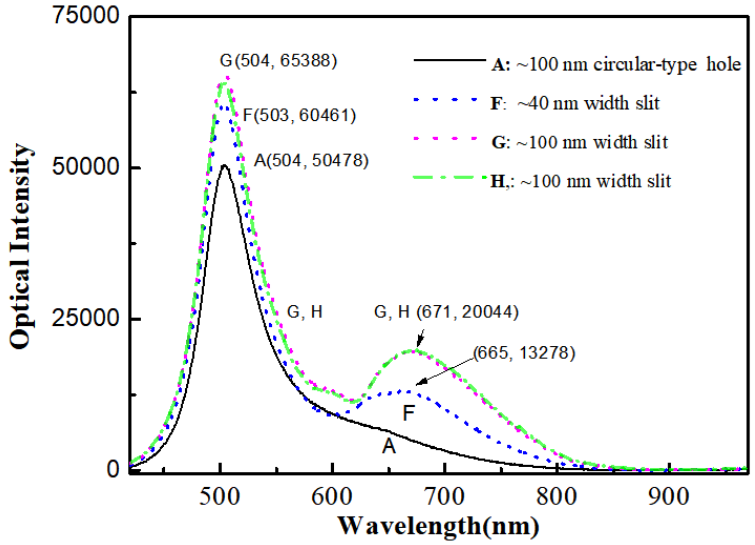

Figure 7. Optical characteristics of the (7x 7) nanoslit array with a 500 nm long single slit with a 100 nm width (G and H) and a ~40 nm width (F). A solid black line (A: a (7x7) circular type aperture array with a single aperture size of (~ 130 nm x ~90 nm)), a dotted blue line (F: 500 nm long and 40 nm wide), a red dash-dot red line (G: 500 nm long and 100 nm width), and a green dash-dotted line (H: 500 nm long and 100 nm wide) are shown.

- Nanopores on pyramids with the aperture sizes ranging from (~ 134 nm x ~ 212 nm) size to (~86.7 nm x ~143 nm) size:

The nano-apertures on the pyramidal array are fabricated using Si microfabrication technique followed by metal deposition as in Fig. 1. Selected 5 TEM images are shown in Figure 8. Inside the dashed yellow circles in Fig. 8(a) and 8(b) and red dotted circle in Fig. 8(c), the white area indicates optically transparent nano-pore region. The formed nano-pores of the sample a3, a4, and a12 is measured to be (23 nm x 18 nm), (62 nm x 42 nm), (26.1 nm x 43.5 nm) on the thin membrane inside the apertures of (86.7 nm x 143 nm), (83.6 nm x 97.1 nm), and (118. nm x 152.7 nm), respectively. The nano-apertures of the sample a15 is measured to be (112.5 nm x 130,4 nm), and the sample a19 has a large aperture with a (212.0 nm x 134.0 nm) size. Considering the fact that the white area contains numerous Au tiny particles on thin Au-C mixture membrane, the white area seems to be a tiny thin, much less than ~10 nm. Au clusters are shown as dark spots around the circumference of the aperture in Fig. 8(b) - Fig 8(d), and numerous Au tiny particles are also presented in the gray area in Fig. 8(e). Au nanoparticles and Au cluster on the gray membrane area can contribute to enhanced optical emission.

Preprints (www.preprints.org) | NOT PEER-REVIEWED | Posted: 5 October 2020 doi:10.20944/preprints202010.0099.v1

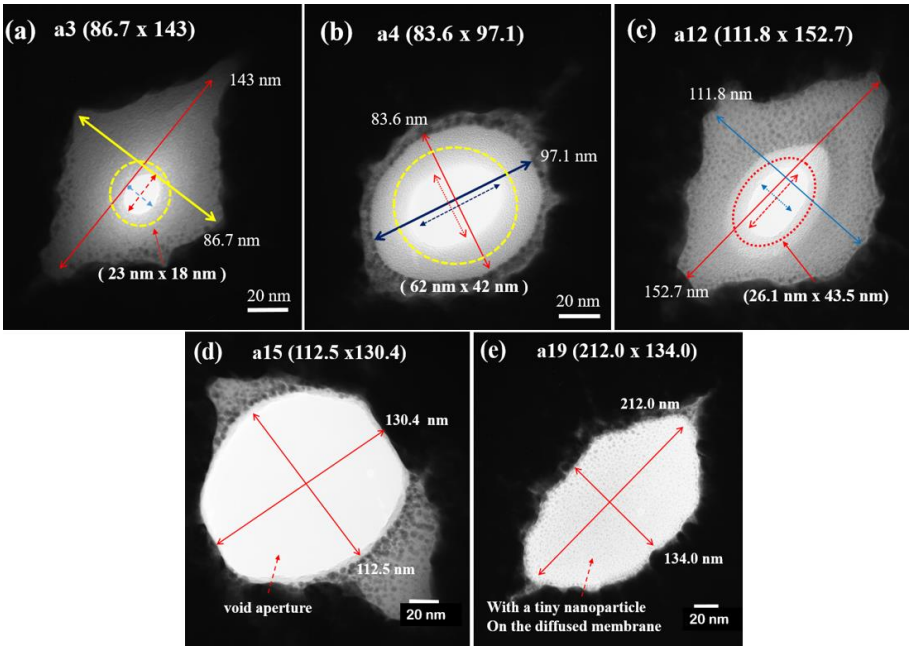

Figure 8. TEM images of nano-pores and nano-apertures on pyramidal apecies with a 200 nm thick Au film. The white pore areas inside the dotted circular area gray membrane are presented in (a), (b) and (c). The pore areas are measured to be (23 nm x 18 nm), (62 nm x 42 nm), and (26.1 nm x 43.5 nm), respectively. The nano-apertures with the sizes of (112.5 nm x 130.4 nm) and (212.0 nm x 134.0 nm) are shown in (d) and (e), respectively. The diffused gray areas are the thin membrane composed with gold and carbon atoms in (d). In addition, the tiny Au particles and clusters are also shown in the diffused dark gray area. However, the white aperture area consists of the tiny Au nanoparticle on the diffused thin membrane in (e).

Table 1 presents the optical output intensity versus wavelengths by using a solid state ND: YAG laser system with a wavelength of 532 nm for a light source and a silicon photo sensor with a 15 mm cone attenuated F filter (spectral range: 400 nm ~ 1064 nm) for photo detection using a Witec SNOM instrument. For the 532 nm input wavelength, the output intensities through the nano-apertures of samples a3, a4, a15, and a19 ranges from 38.6 μW to 48.3 μW. The ratios for the samples a3, a4, a15, and a19 are order of ~ 3.1 x 10^{-2}, 3.1 x 10^{-2}, 2.6 x 10^{-2}, 3.3 x 10^{-2}, respectively. For the 780 nm input wavelength, the output intensities through the nano-apertures of samples a3, a4, a15, and a19 are measured to be 8.4 μW, 7.7 μW, 6.7 μW, 14.3 μW, respectively. And the corresponding ratios would be 0.36 x 10^{-2}, 0.33 x10^{-2}, 0.28 x10^{-2}, and 0.60 x10^{-2}, respectively. The differences could be attributed to the higher excitation of photons at 532 nm input wavelength than at 780 nm, and to the spp-mediated emission with its peak at ~ 500 nm.

Preprints (www.preprints.org) | NOT PEER-REVIEWED | Posted: 5 October 2020 doi:10.20944/preprints202010.0099.v1

Table 1. Optical characteristics of the fabricated Au nano-apertures with its sizes for the a3 (~143 nm x 86.7 nm), a4(83.6 nm x 97.1 nm), a15 (112.5 nm x 130.4 nm), and a19 (134.0 nm x 212.0 nm) are presented for the input wavelengths of 532 nm and 780 nm.

Sample ID	aperture size (nm^2)	Input wavelength (nm)	Input Intensity ($\circledcirc W/cm^2$)	Output Intensity ($\circledcirc W/cm^2$)	I_{out}/I_{in} ($x10^{-2}$)
a3	143 x 86.7	532	1477	45.7	3.1
a4	83.6 x 97.1			42.0	3.1
a15	120.0 x 130.4			38.6	2.6
a19	134.0 x 212.0			48.3	3.3
a3	143 x 86.7	780	2366	8.4	0.36
a4	83.6 x 97.1			7.7	0.33
a15	120.0 x 130.4			6.7	0.28
a19	134.0 x 212.0			14.3	0.60

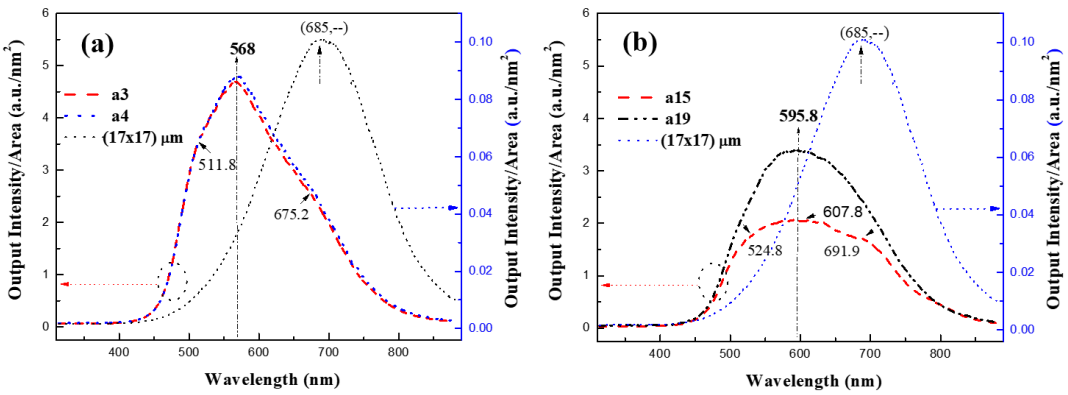

Figure 9. Normalized output optical intensities for Au apertures with visible optical Gaussian peaks around ~ 685 nm. For the Au apertures of the a3 sample and a4 sample, the output spectra centered around at ~568 nm and 569 nm, along with a relatively sharp and narrow Gaussian-type shape spectra are presented in (a). Both transmitted optical profiles of sample a3 and sample a4 have optical peaks at 568 nm with two points of inflection; One point of inflection at 511.8 nm, and another point of inflection at 675.2 nm. For the a19 sample, the output optical peak around ~ 595.8 nm with broadened Gaussian shape between ~ 500 nm and ~ 700 nm are presented. For the sample a15, the profile has a center at 607.8 nm with a broadband between 524.8 nm and 691.9 nm. Input beam optical intensity was calibrated using through the (17 μmx 17 μm) aperture

Preprints (www.preprints.org) | NOT PEER-REVIEWED | Posted: 5 October 2020 doi:10.20944/preprints202010.0099.v1

The optical output intensity versus wavelength for the samples of a3, a4, a15, and a19 are presented in Figure 9. Optical characterization was performed by using Nikon Optical Eclipse Ti-U microscope with Princeton Instruments spectrophotometer (Acton SpectroPro 2300i, 150g/ mm). Input optical Gaussian beam intensity was calibrated by using a (17 μm x 17 μm) square Si aperture. Output beam intensity profiles from the sample a3 and the sample a4 are presented in Fig. 9(a). The areas of these particular samples of a3 and a4 are very close to each other, 7820 nm^2 and 6680 nm^2, respectively, and the ratio versus wavelength optical spectra are exactly identical. In addition, even with the 532 nm wavelength laser measurements, the ratios of the output to the input intensity are also same; 3.1 x 10^{-2}. We observed the similar results from the sample a12, and a14 [Supplementary material 1]. Two optical beam profiles have optical peaks at 568 nm and two inflection points; one at 511.8 nm and another one at 675.2 nm. One point of inflection at 511.8 nm may be attributed from the intraband transition emission, and another point of inflection at 675.2 nm could be attributed from spp-coupled incoming wave via nano-aperture. For the sample a19, the output optical peak around ~ 595.8 nm with a broadened Gaussian shape between ~ 500 nm and ~ 700 nm are presented. The optical profile of the sample a15 has a center point at 607.8 nm with a broadband between 524.8 nm and 691.9 nm. At least, our optical profile broadening with increased aperture size is agreeable with the previously published results [23, 24].

The ratio of the output intensity to the input intensity can provide the information for the nano-apertures and the optical characteristics of the materials. Figure 10 presents the ratio of the normalized output intensity to the normalized input intensity versus wavelength. The sharp conical ratio profiles with the optical peaks at 497 nm and 499 nm for the sample a3 and a4, respectively, are shown with slightly deviated to the right wavelength from the peak line at 497 nm. The asymmetrical profile is clearly presented; At the ratio value of 150, close to the half maximum, the corresponding wavelengths are 467.6 nm and 551.1 nm, not symmetrical from the peak. For the samples a15 and a19, the profiles became broader and asymmetrical with the peak around ~ 500 nm. This asymmetrical profile may be attributed to the contribution from the spp-coupled wave with the incoming beam through the aperture.

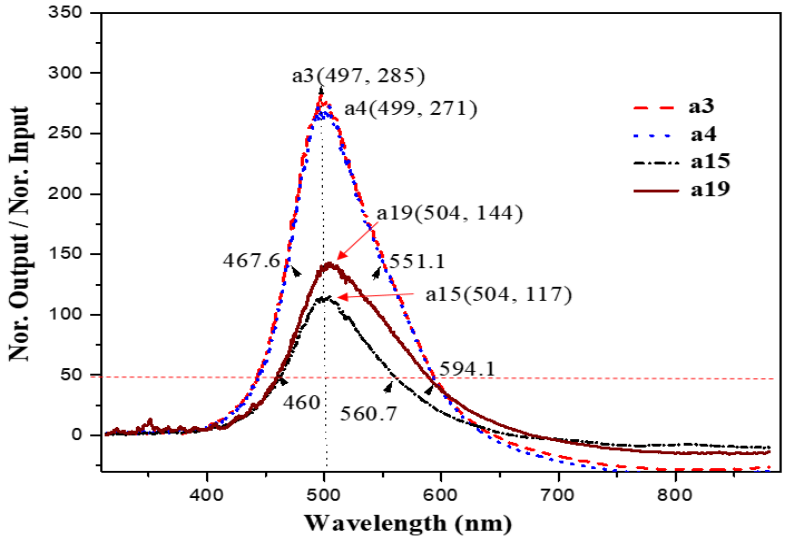

Figure 10. Ratios of the normalized output intensity to the normalized input intensity versus wavelength for the sample a3, a4, a15, and a19 are presented. For the sample a3 and the sample a4, the ratio profiles are a conical shape profile centered around ~497 nm and 499 nm, respectively. With a15 and a19 samples, the ratio profiles present lower maxima with wider full width half maximum (FWHM) than with a3 and a4 samples.

Preprints (www.preprints.org) | NOT PEER-REVIEWED | Posted: 5 October 2020 doi:10.20944/preprints202010.0099.v1

- Fabrication of (7 x7) nanoslit array with a (~ 10 nm width x ~ 300 nm length) slit

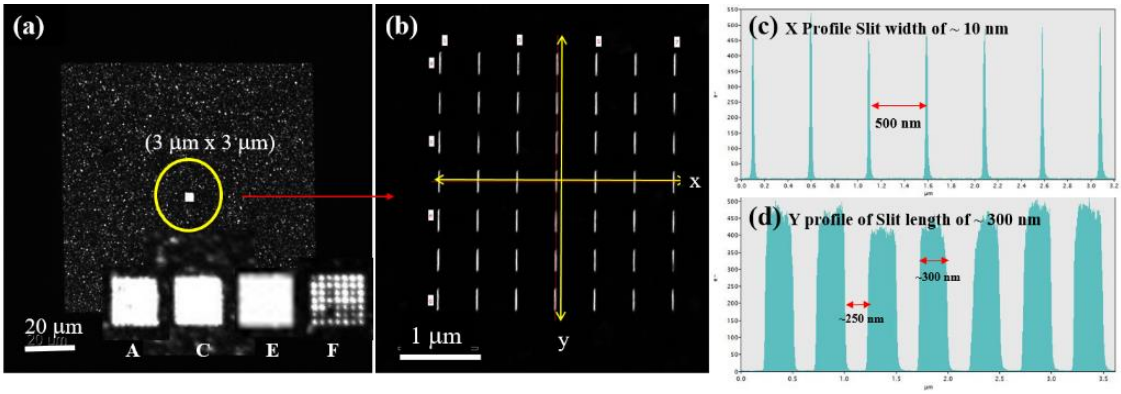

Figure 11. TEM images of the (~100 μm x ~100 μm) membrane and the (7 x 7) nanoslit array with (~3 μm x ~3 μm) at the center of the A, C, E, and F membrane (inside a solid yellow circle) are presented. The 3 white squares at the bottom indicate the nanoslit areas of A, C, and E membranes, and the gray square area with grids indicates the nanoslit in F membrane. The (x, y) profiles at the electron beam detector were measured. The widths and the length of the slits are found to be ~ 10 nm and ~300 nm, respectively. The (x, y) pitches of the slit arrays are found to be (~500 nm, ~250 nm) in (c) and (d).

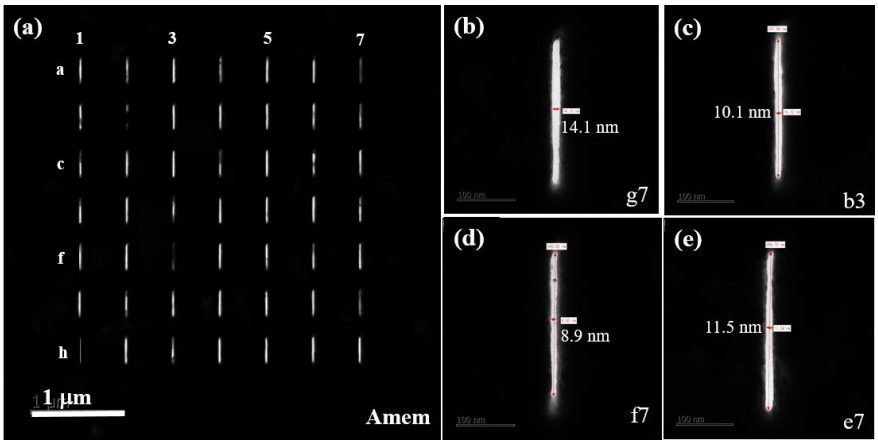

Figure 12. TEM images of the sample A membrane for a (7x7) nanoslit array., Several dimmy nanoslits are also shown due to Au atoms diffusion during 30 keV Ga ion beam drilling. Widths from slits (g7, b3, f7, and e7) are measured to be 14.1 nm, 10.1 nm, 8.9 nm, and 11.5 nm, respectively.

Preprints (www.preprints.org) | NOT PEER-REVIEWED | Posted: 5 October 2020 doi:10.20944/preprints202010.0099.v1

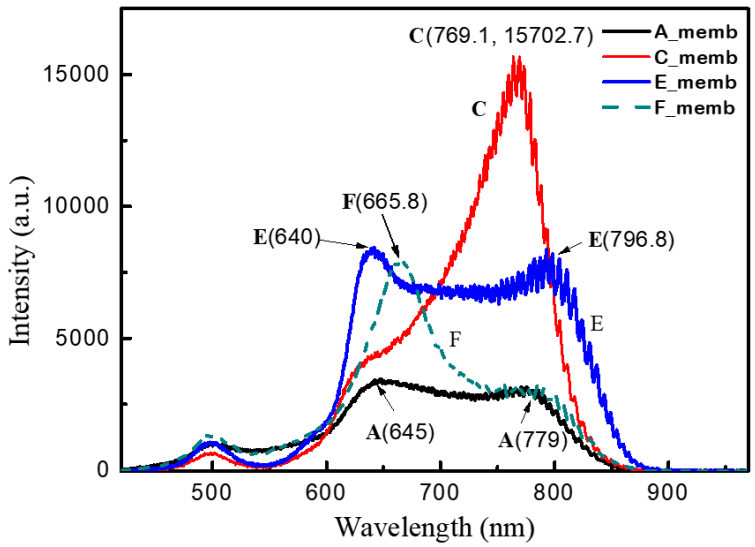

Figure 13. Optical characteristics of the (7 x7) slit arrays are presented. Optical emission spectra ranging from ~ 450 nm to ~900 nm are shown along with a small emission peak at ~ 500 nm. Two optical emission spectra from the sample A and the sample E present relatively flat broad bands (plateau region) from ~ 640 nm to ~ 800 nm. A strong emission peak at 665.8 nm from the sample F (blue line), and a sharp peak at 769.1 nm from the sample C (red line) can be attributed to contribution from the transmitted beam through the hole on the F membrane, and scattering from ~ 200 nm Au particle on the C membrane, respectively.

The (7x7) nanoslit arrays are fabricated by using 30 keV Ga ion FIB on the 200 nm thick Au on the supporting layer 20 nm SiN. Figure 11 (a) presents TEM images of the (~100 μm x ~100 μm) membrane and the (7 x 7) nanoslit array with (~3 μm x ~3 μm) at the center of the A, C, E, and F membrane (inside a solid yellow circle) are presented. The (x, y) pitch is measured to be (500 nm, 250 nm) in Figure 11(b) and Figure 11(c). The size of each nanoslit is measured to be (~ 10 nm opening wide x ~ 300 nm long). TEM images for the E membrane are shown [supplementary material 2]. A FESEM image of a ~ 200 nm size Au particle on the C membrane and a TEM image of the (~7.2 μm x ~2.3 μm) size aperture on the F membrane are presented [supplementary material 3]. The measured optical characteristics for the 4 samples are presented in Figure 13. The optical spectra ranging from ~ 450 nm to ~900 nm are shown along with a small Gaussian shape emission peaks at ~ 500 nm. Two broad emission bands from the sample A and the sample E exhibit relatively flat broad bands with a plateau region from ~ 600 nm to ~ 850 nm, even though the emission band from E has greater intensities by double than those from the sample A. This can be attributed from the different surface status between two samples. The green strong peak at F (665.8) may be attributed to the spp-coupling contribution from the small void aperture (~ 7.2 μm x ~2.3 μm) on the membrane. A red sharp peak at C (769.1) can be attributed to the spp scattering from a ~ 200 nm size Au particle.

4. Discussion and Conclusion

(i) We investigated influence of the high energy electron beam irradiation dependent on the aperture size. For the aperture greater than aperture thickness, a 2 keV FESEM electron beam irradiation was utilized, then electron beam irradiation at 3 pA, 300 keV TEM was followed to obtain a nanopore of ~ 4 nm. For a (56.2 nm x 33.1 nm) Au aperture on a 200 nm thick Au film, much higher electron beam currents of ~60 pA or more at 200 keV TEM were irradiated to obtain the Au nanopore with its size of (8.3 nm x15.3 nm). With the higher currents greater than 100 pA at 200 keV, pore closing and

Preprints (www.preprints.org) | NOT PEER-REVIEWED | Posted: 5 October 2020 doi:10.20944/preprints202010.0099.v1

thinning of the formed membrane are observed due to diffusion of gold atoms and carbon atoms, sputtering of carbon atoms, and evaporation of Au atoms.

(ii) In order to investigate the nanoscale surface plasmon interference and the spp-mediated intraband emission, we fabricate the nanoscale double slits dependent upon the slit opening and slit pitch. For a 200 nm slit opening, we only observed one strong optical peak around ~ 666.5 nm, however, for a 50 nm slit opening, the strong optical emission peaks around ~ 500 nm are observed possible due to spp-mediated intraband emission. Another optical peaks around ~700 nm are shown. This can be attributed to spp-coupling interference with the input beam whose peak is around ~ 665.5 nm.

(iii) Au nanopores and apertures on the pyramidal apecies with optical characterizations.

Au pyramidal-apertures with its sizes ranging from (143 nm x 86.7 nm) to (134 nm x 212 nm) were micro-fabricated). The observed output intensity peaks for the relatively small aperture areas of a3(143 nm x 86.7 nm) and a4(83.6 nm x 97.1 nm) and for the greater areas of samples a15(112.5 x 130.4 nm) and a19(134.0 nm x 212.0 nm), are observed to be at 568.2 nm and 569.2 nm, and at 596.5 nm and 592.7 nm, respectively. The full width half maxima(FWHM) for the optical spectra from the a3 sample and the a4 sample is much narrower than those for the sample a15 and the sample 19. The greater FWHM with the shifted peak to the higher wavelengths indicates the coupling with incoming wave. In addition, the ratio profiles also present the strong contribution from the spp-mediated intraband emission at ~500 nm. The exactly same optical emission spectra along with the ratio profiles from sample a3 and the sample a4 can be attributed to Lord Raleigh's statement about the diffraction small particle and Babinet principle; the farfield emission does not depend upon the shape of the particle and the aperture for the small particle and aperture smaller than the wavelength.

(iv) Optical characterization of the fabricated optical platforms with a (7x7) nanoslit array, or with a circular type hole with a (90 nm x 130 nm) size on the 130 nm thick Au film; Regardless of the aperture types, either circular or slit, strong sharp optical peaks around~ 500 nm are observed. For the nanoslit array with a slit dimension of (~ 100 nm x ~ 500 nm), a sharp conical type profile with its peak around ~ 500 nm and a broad profile with a small peak around ~ 671 nm are observed. Even though a strong sharp conical shape profile with its peak at ~ 500 nm is presented for the nanoslit array with a slit dimension of (~ 40 nm x ~ 500 nm), a smaller broad profile at 665 nm is shown. No optical emission peak around ~ 670 nm is observed for this sample; a (7x7) circular type array fabricated on the ~ 130 nm thick Au membrane, with its typical aperture dimension of (~130 nm x ~90 nm).

(v) We have optically characterized the fabricated pyramidal nanopores and nanometer size apertures. For the small nanopores and apertures of the sample a3 and the sample a4 with, the conical type output optical profiles present its peak at 568 nm, however, for the larger apertures of the sample a15 and the sample a19, the broad profiles are shown with the shifted peak position at 595.8 nm from input peak at 685 nm. The peak shift can be attributed to spp-coupling from incoming optical beam through the nano-apertures and the possible scattering with Au particles and Au clusters. The detailed physical mechanism is further to be investigated.

(vi) The broad optical spectra ranging from 550 nm to 900 with a small optical peak at 500 nm was obtained from the (7 x 7) nanoslit array platforms, possibly contributed from the spp-mediated intraband emission. The fabricated (7 x7) nanoslit array consists of each slits with a (~10 nm x ~300 nm) size. The (x, y) pitch of the slit array is measured to be (250 nm, 500 nm). The *small optical peak at 500 nm* can be attributed to *spp-mediated intraband emission*. *The broad emission in the visible range can be due to interband transitions of d-band electrons into the conduction band*, and *the emission in the infrared region is generated from intraband transitions mediated by the strongly confined fields (localized surface plasmons)* from the nano-slit array with a ~ 10 nm slit opening.

5. Conclusions

 doi:10.20944/preprints202010.0099.v1

We fabricated Au nanopores on the pyramids and various Au nano-aperture platform with optical characterizations.

● Depending upon the aperture thickness and aperture diameter, pore-formation procedures are varied; *For the aperture thickness smaller than the aperture diameter*, two step processes for pore formation were carried out; an electron beam irradiation by using 2 keV, 1.4 nA FESEM followed by successive electron beam irradiations at 3 pA, 300 keV TEM was performed to form the nanopore with a few nanometer diameter on the diffused Au-C mixed membrane. *For the aperture thickness greater than the aperture diameter*, a ~60 pA electron beam irradiation at 200 keV TEM were performed to obtain a controllable nanopore down to a few nanometer. Under electron beam irradiations at 200 keV with a high beam current of ~ 100 pA or greater, shrinking of nanopore, diffusion of gold atoms, followed by Oswald ripening, and thinning of the membrane due to evaporation and sputtering of Au and C atoms were observed.

● Optical emission from the various Au nanostructures depending upon the film thickness and aperture size; (i) For the nanoscale double slit on the ~ 200 nm thickness with a slit opening of ~ 200 nm, no optical peaks at ~ 500 nm is observed. However, for the slit opening of ~ 50 nm, the strong optical peak at ~ 500 nm are observed in addition to the spp-coupled peak around ~700 nm. With decreasing the thickness down to ~ 130 nm, the sharp optical profile with the peaks at 500 nm are observed regardless of the slit aperture and circular-type aperture. The optical emission profile with its peak at 500 nm can be attributed to the spp-mediated intraband transition.

● Optical emission profiles from the nanopores and the nano-apertures on the 200 nm thick Au pyramid; The emission profiles show strong contribution from spp-mediated intraband for the small apertures, and weak contribution from spp-coupled transition for larger apertures. The ratio profiles (normalized output intensity to normalized input intensity) versus wavelength present the sharp profiles centered at ~500 nm. With decreased aperture diameter, the increased backward scattering along the pyramidal surface would result in the enhanced spp-mediated intraband emission.

● Observation of the broad emissions from visible to infrared region: These phenomena can be attributed to the followings; visible emission from the *interband transitions of d-band electrons into the conduction band, and infrared emission* from *intraband transitions mediated by the strongly confined localized surface plasmons. These finding can be utilized as a nanosensor device for single molecule detection and self-cooling thermal device by using infrared emission characteristics.*

Author Contributions: "Conceptualization, Choi, S.S.(nanofabrication); Kim, K.J. (single molecule detection); Park, M.J.(plasmonics); methodology, Bae B.S. (materials preparation); Kim, H.T.; Choi, S.B.; formal analysis, Choi, S.S.; Kim, H.T.; investigation, Choi, S.S.; resources; data curation, Byung Seong Bae, Yong Min Lee.; writing—original draft preparation, Choi, S.S.; writing—review and editing, Bae, B.S.; Park, M.J.; Lee, Y.M.

Funding: This work was supported by the research funding programs (Development of Biofriendly Optical Nanopore, 2018R1D1A1B07050106) under the Basic Science Research Program through the National Research Foundation (NRF) funded by the Ministry of Education, Science and Technology, South Korea.

Acknowledgments: This work was supported by the research funding programs (Development of Biofriendly Optical Nanopore, 2018R1D1A1B07050106) under the Basic Science Research Program through the National Research Foundation (NRF) funded by the Ministry of Education, Science and Technology, South Korea.

Conflicts of Interest: The authors declare no conflict of interest.

 doi:10.20944/preprints202010.0099.v1

References

1. Muthukumar, M.; Plesa, C.; Dekker, C. Single-molecule sensing with nanopores. *Phys. Today*. **2015**. 68, 40-48.
2. Ebbesen, T.W., Lezec, H.J., Ghaemi, H.F., Thio, T., Wolff, P.A. Extraordinary optical transmission through sub-wavelength hole arrays. *Nature*, **1998,** 391, 667-669.
3. Choi, S.S., Park, M.J., Han, C.H., Kim, Y.S., Park, N.K., Han, S.H., Choo, H. Fabrication of pyramidal probes with various periodic patterns and a single nanopore. *J. Vac. Sci. Technol B***. 2015**. 33, 06F203.
4. Choi, S.S., Oh, S.J., Han, S.H., Park, N.K., Kim, Y.S., Yoo, J.H., Park, K.J. Formation of an Au membrane incorporated with carbon atoms under electron beam irradiations. *Surf. Coating. Technol.* **2016,** 306**,** 113-118.
5. Choi, S.S., Park, M.J., Yamaguchi, T., Han, C.H., Oh, S.J., Kim, S.I., Park, K.J., Yoo, J.H., Kim, Y.S., Park, N.K. Nanopore formation on Au coated pyramid under electron beam irradiations (plasmonic nanopore on pyramid). *Sens. Bio-Sens. Res.* **2016,** *7*, 153-161.
6. Choi, S.S., Park, M.J., Yamaguchi, T., Kim, S.I., Park, K.J., Park, N.K. Fabrication of nanopore on pyramid. *Appl. Surf. Sci.* **2014,** 310, 196-203.
7. Choi, S.S., Oh, S.J., Han, C.H., Park, D.J., Choi, S.B., Kim, Y.S., Park, N.K. Au cluster formation on a pore-containing membrane under various surface treatments. *J. Vac. Sci. Technol B*. **2017,** 35, 04F107.
8. Komoda, T. Study on the Structure of Evaporated Gold Particles by Means of a High Resolution Electron Microscope. *J. Phys. Soc. Jpn.* **1968**, 7, 27-30.
9. Pashlemy, D.W.; Stowellm, J.; Jacob, H.; Law, T.J. The growth and structure of gold and silver deposits formed by evaporation inside an electron microscope, *Philos. Mag*. **1964**, 10, 127-157.
10. Ino, S. Epitaxial Growth of Metals on Rocksalt Faces Cleaved in Vacuum. II. Orientation and Structure of Gold Particles Formed in Ultrahigh Vacuum. *J. Phys. Soc. Jpn.* **1966**, 21, 346-362.
11. Martin, T. P. Shells of atoms. *Phys. Rep*. **1996**, 273, 199-241.
12. Buffat. Ph.; Borel, J. P. Size effect on the melting temperature of gold particles. *Phys. Rev. A*. **1976**, 13, 2287-2298.
13. Li, H.; Li, L.; Pedersen, A.; Gao, Y.; Khetrapal, N.; Jonsson, H.; Zeng, X.C. Magic-number gold nanoclusters with diameters from 1 to 3.5 nm: Relative Stability and Catalytic Activity for CO Oxidation. *Nano Lett.* **2015,** 15, 682-691.
14. Schmitt, M.; Kusche, R.; Issendorff, B.V.; Haberland, H. Irregular variations in the melting point of size-selected atomic clusters. *Nature* **1998**. 393, 238-240.
15. Storm, A.J.; Chen, J.H.; Ling, X.S.; Zanbergen, H.W.; Dekker, C. Fabrication of solid-state nanopores with single-nanometre precision. *Nat. Mater*., **2003**, 2, 537–540.
16. Li, J.; Stein, D.; McMullan, C.; Branton, D.; Aziz, M.J.; Golovchenko, J. A. Ion-beam sculpting at nanometre length scales. *Nature* **2001.** 412. 166-169.
17. Schouten, H. F.; Kuzmin, N.; Dubois, G.; Visser, T. D.; Gbur, G.; Alkemade, P.F.A.; Blok, H.; Hooft, G.W.'t.; Lenstra, D.; Eliel, E.R. Plasmon-Assisted Two-Slit Transmission: Young's Experiment Revisited. *Phys. Rev. Lett*. **2005,** 94, 053901.
18. Gan, C. H.; Gbur, G.; Visser, T. D. Surface plasmons modulate the spatial coherence in Young's interference experiment. *Phys. Rev. Lett.* **2007**, 98, 043908.
19. Verma, M.; Joshi, S.; Bisht, N. S.; Kandpal, H. C.; Senthilkumaran, P.; Joseph, J. Effect of surface plasmons on spectral switching of polychromatic light with Au-double-slit. *J. Opt. Soc. Am.* **2012**, 29, 195-199.
20. Choi, S.S.; Park, M.J.; Han, C.H.; Oh, S.J.; Kim, H.T.; Choi, S.B.; Kim, Y.S. Plasmonic Nanopore Fabrication for Single Molecule Bio Sensor Using Electron Beam Irradiation. ECS Trans. 2018, 85, 69-76.
21. Choi, S.S.; Oh, S.J.; Lee, Y.M.; Kim, H.T.; Choi, S.B.; Bae, B. S. Fabrication of Plasmonic Optical Nanopore Platform for Single Molecule Sensing. J. Electrochem. Soc. 2020. 167, 027503.
22. S.S. Choi, M.J. Park, Y.M. Lee, B.S. Bae, H. T. Kim, S.B. Choi, Fabrication of the Au Nano-Aperture Array Platform for Single Molecule Analysis. ECS J. Solid State Sci. Technol. 2020. 9. 115015.
23. Obermüller C.; Karrai, K. Far field characterization of diffracting circular apertures, Appl. Phys. Lett. **1995,** 67, 3408-3410.

24. Drezet, A.; Woehl,J.C.; Huant, S. Diffraction by a small aperture in conical geometry: Application to metal-coated tips used in near-field scanning optical microscopy, Phys. Rev. E. **2002**, 65, 046611.
25. Lord Rayleigh, On the passage of waves through apertures in plane screens and allied problems, Phil. Mag. 1987, XLIII, 259–272.
26. Babinet, M.; Mémoires d'optique météorologique," C. R. Acad. Sci. 1837. **4**, 638–648.
27. Gao, H.; Hensie, J.; Odom, T.W. Direct Evidence for Surface Plasmon-Mediated Enhanced Light Transmission through Metallic Nanohole Array. *Nano Lett.* **2006**, 6, 2104–2108.
28. Beversluis, M.R.; Bouhelier, A.; Novotny, L. Continuum generation from single gold nanostructures through near-field mediated intraband transitions. *Phys. Rev. B*. **2003**, 68, 115433.
29. Ebrahimpour, Z.; N. Mansour, N. Plasmonic Near-Field Effect on Visible and Near-Infrared Emissions from Self-Assembled Gold Nanoparticle Films. *Plasmonics*, **2018**,13,1335-1342.
30. Greffet, J.J. Revisiting thermal radiation in the near field, *C. R. Phys.* **2017**, 18, 24-30.
31. Baranov, D.G.; Xiao, Y.; Nechepurenko, I. A.; Krasnok, A.; Alù A.; Kats, M.A. Nanophotonic engineering of far-field thermal emitters. *Nat. Mater.* **2019**, 8, 920–930